Supplementary Information (SI) for Inorganic Chemistry Frontiers.

Supporting Information

A Bis-Aromatic MOF System Constructed by a Copper Iodine Cluster and Porphyrinic Ligand for Enhancing Near-Infrared Photothermal Conversion

Man Cao, Qian-You Wang, Run-Meng Li, Fangfang Dai, Shan Wang, Peng Luo, Jia-Hua Hu,* Xi-Yan Dong and Ren-Wu Huang*

Supplementary Text

Materials and Methods

All reagents and solvents were purchased from commercial sources and used without further purification. Single-crystal X-ray diffraction (SCXRD) was performed on a Rigaku XtaLAB Synergy Custom using Cu Kα radiation. Powder X-ray diffraction (PXRD) patterns of the samples were obtained in the range of 3-50° on a Riguku D/Max-2500PC X-ray diffractometer. The optical absorption and diffused reflectance spectra were obtained on a Hitachi UH4150 spectrophotometer. The photoluminescence (PL) emission spectra were measured by using a Horiba FluoroLog-3 spectrofluorometer. The 1064 nm power-adjustable laser was used for irradiation in both photothermal experiments and photothermal antibacterial experiments, with temperature changes recorded using a FOTRIC infrared thermal imager. The *in-situ* Raman spectra were recorded on a lab RAM HR Evolution-HORIBA using a 532 nm laser as the excitation source. The femtosecond transient absorption (fs-TA) data were recorded on a modified pump-probe spectrometer (Helios Fire, Ultrafast Systems LLC) in combination with an ultrafast laser system (Coherent) using a 360 nm pump. The live-dead bacterial imaging was obtained using a Leica TCS SP8 confocal fluorescence microscope (CLSM). Scanning electron microscopy (SEM) images were obtained using a Zeiss Sigma 500.

Reactive Oxygen Species (ROS) Measurement

Detection of $^1O_2$ generation：9,10-Dimethylanthracene (DMA) functions as a fluorescent probe suitable for the detection of $^1O_2$ generation in EtOH. Typically, 2 mg of DMA was dissolved in 4 mL of EtOH with **TPyP** (1.23 mg, 2 μmol porphyrin unit), **$Cu_{14}I_{14}$-CuTPyP** (4.03 mg, 2 μmol porphyrin unit) or **Cu-CuTPyP** (1.94 mg, 2 μmol porphyrin unit) under white LED light irradiation (80 mW cm^{-2}). The experimental outcomes were monitored through the decay of fluorescence emission peaks, specifically at wavelengths of 430 and 451 nm (ex: 300 nm).

Fluorescence Measurement

The fluorescence steady-state emission spectra of **TPyP** (0.04 M), C**u-CuTPyP** (0.04 M), and **$Cu_{14}I_{14}$-CuTPyP** (0.04 M) dispersed in EtOH were recorded using a Horiba FluoroLog-3 spectrofluorometer, and the photoluminescence quantum yield of the dispersions was measured with an integrating sphere using 400 nm excitation, with ethanol serving as the blank reference.

Theoretical calculations

Electronic localization function (ELF) calculations were performed within the framework of the density functional theory (DFT) as implemented in the Vienna Ab initio Software Package (VASP 5.3.5) code, with the Perdew-Burke-Ernzerhof (PBE) generalized gradient approximation and the projected augmented wave (PAW) method.[1] The cut-off energy for the plane-wave basis set was set to 400 eV. The Brillouin zone of the bulk unit cell was sampled by Monkhorst-Pack (MP) grids for **$Cu_{14}I_{14}$-CuTPyP** optimizations.[2] The **$Cu_{14}I_{14}$-CuTPyP** was determined by a 1 × 1 × 1 Monkhorst−Pack grid. The convergence criterion for the electronic self-consistent iteration and force was set to 10^{-5} eV and 0.01 eV/Å, respectively.

The results of nucleus-independent chemical shift (NICS) and simulated Raman vibration spectra were calculated by DFT with Gaussian under PBE1PBE functional. Def2SVP was used to calculate C, H, N, Cu and I atoms. The initial model for ground state optimization was chosen to be a single crystal structure. Since no negative eigenvalues were observed in the vibration frequency analysis, it can be concluded that all the reported static points represent true minima.

Calculation of the photothermal conversion efficiency

The photothermal conversion efficiency of the **$Cu_{14}I_{14}$-CuTPyP** was determined by monitoring the temperature change of quartz glass (d = 1.0 cm, 340 mg) coated with **$Cu_{14}I_{14}$-CuTPyP** powders, while continuously irradiated with a 1064 nm laser (0.5 W cm^{-2}) until the glass reached a stable temperature state, and then cooled in the ambient environment over time. The conversion efficiency was determined according to

previous method.[3] Details are as follows:

Based on the total energy balance for this system:

$$\sum_i m_i C_{p,i} \frac{dT}{dt} = Q_S - Q_{loss}$$

where m_i (0.34 g) and $C_{p,i}$ (0.8 J (g °C)$^{-1}$) are the mass and heat capacity of system components (**$Cu_{14}I_{14}$-CuTPyP** samples and quartz glass), respectively. Q_s is the photothermal heat energy input by irradiating NIR laser to **$Cu_{14}I_{14}$-CuTPyP** samples, and Q_{loss} is thermal energy lost to the surroundings. When the temperature is maximum, the system is in balance.

$$Q_S - Q_{loss} = hS\Delta T_{max}$$

where h is heat transfer coefficient, S is the surface area of the container, ΔT_{max} is the maximum temperature change. The photothermal conversion efficiency η is calculated from the following equation:

$$\eta = \frac{hS\Delta T_{max}}{I\left(1 - 10^{-A_{1064}}\right)}$$

where I is the laser power (0.5 W cm^{-2}) and A_{1064} is the absorbance of the samples at the wavelength of 1064 nm (0.658).

In order to obtain the hS, a dimensionless driving force temperature, θ is introduced as follows:

$$\theta = \frac{T - T_{surr}}{T_{max} - T_{surr}}$$

where T is the temperature of **$Cu_{14}I_{14}$-CuTPyP**, T_{max} is the maximum system temperature (80.0 °C), and T_{surr} is the initial temperature (25.2 °C).

The sample system time constant τ_s

$$\tau_s = \frac{\sum_i m_i C_{p,i}}{hS}$$

thus $\frac{d\theta}{dt} = \frac{1}{\tau_s} \frac{Q_s}{hS\Delta T_{max}} - \frac{\theta}{\tau_s}$

when the laser is off, $Q_s = 0$, therefore $\frac{d\theta}{dt} = -\frac{\theta}{\tau_s}$, and $t = -\tau_s \ln \theta$

so hS could be calculated from the slope of cooling time vs $\ln\theta$. Therefore, τ_s is 59.04 s (Fig. 2f) and the photothermal conversion efficiency η is 63.77%.

Similarly, **TPyP** and **Cu-CuTPyP** showed photothermal conversion efficiencies of 35.70% and 57.70%, respectively, using the above method.

Photothermal antibacterial activity study

Gram-negative bacteria (Escherichia coli (*E. coli*), ATCC 8739) and Gram-positive bacteria (Staphylococcus aureus (*S. aureus*), ATCC 6538) were used as model strains for the study. All vessels and materials were sterilized in an autoclave before the experiments. The bacterial cells were grown in Luria-Bertani (LB) broth at 37 °C for 18 h to yield a cell count of approximately 10^9 CFU mL^{-1}. Then, the bacterial cells were collected by centrifugation (5000 rpm for 5 min) and resuspended in a sterile saline solution (0.9% (w/v)). The bacterial concentration for the bactericidal study was 10^6 CFU mL^{-1}, which was adjusted by the gradient dilution method using 0.9% (w/v) saline solution.

Typically, 100 μL of bacterial suspension (*E. coli* or *S. aureus*, 10^6 CFU mL^{-1}) is sprayed onto the surface of **$Cu_{14}I_{14}$-CuTPyP@PVDF** film, **PVDF** film, **TPyP@PVDF** film, or **Cu-CuTPyP@PVDF** film (each with a size of 1 × 1 cm^2), respectively, and then irradiated with a 1064 nm laser (0.2 W cm^{-2}) for 10 minutes. Next, the above-mentioned films are thoroughly washed with 900 μL of 0.9% (w/v) saline solution, and then 100 μL of the wash solution is taken and diluted with a tenfold gradient to obtain different concentrations of the dilution solution. The residual bacterial concentrations are determined by the standard plate count method.

The photothermal antibacterial efficiency of different films was calculated using the following equation:

$$Antibacterial\ Efficiency = \frac{C_0 - C}{C_0}$$

In this equation, "C_0" (CFU) represents the initial number of bacterial colonies before photothermal antimicrobial testing, and "C" (CFU) represents the number of bacterial colonies after photothermal antimicrobial tests. The different films were tested for their photothermal antibacterial efficacy against *E. coli* and *S. aureus* under 1064 nm light (0.2 W cm^{-2}) for 10 minutes.

All antibacterial experiments were conducted three times independently, and the results were expressed as the average value with error bars representing the maximum positive and negative deviations.

Live/Dead Cell Fluorescence Assay

0.9% (w/v) saline solution were collected by centrifugation with 8000 rpm respectively. The collected bacteria cells were stained in dark by incubating with SYTO 9 and PI together for 30 min. Then, 10 μL of bacterial solution was dropped onto a glass slide. Confocal images were taken with LEICA TCS SP8 STED fluorescence confocal microscopy system (excitation: 488 and 552 nm).

Analysis of bacterial morphologies

Treat bacterial cultures with the desired method, like photothermal disinfection using **$Cu_{14}I_{14}$-CuTPyP@PVDF** film. Fix the bacteria in 2.5% glutaraldehyde, wash them with PBS buffer three times, and dehydrate through increasing ethanol concentrations (30%, 50%, 70%, 85%, 95%). Suspend the bacteria in heavy ethanol, drop them onto a silicon wafer, then mount the wafer onto SEM stubs with conductive adhesive. Then, coat with a thin layer of gold. Finally, the morphologies of the bacteria were analyzed using SEM.

Preparation of crystals

Synthesis of **$Cu_{14}I_{14}$-CuTPyP:**

CuI (15 mg, 0.079 mmol) was stirred in CH_3CN (4 mL) and ethylene glycol (60 μL). Then, TPyP (3 mg, 0.0048 mmol), CF_3COOH (20 μL, 1.2 mmol), and N_2H_4 (85% solution in water, 10 μL) were sequentially added. After stirring the mixture for 5 minutes, it was placed in an 80 °C oven for three days, resulting in the formation of dark purple diamond-shaped crystals of **$Cu_{14}I_{14}$-CuTPyP** (48.22% yield based on TPyP). Elemental analysis (%) for evacuated **$Cu_{14}I_{14}$-CuTPyP** ($C_{80}H_{48}Cu_{16}I_{14}N_{16}$, M = 4026.74): calcd. C: 23.86, H: 1.19, N: 5.57; found C: 24.11, H: 1.15, N: 5.49.

Synthesis of **Cu-CuTPyP:**

$(CH_3COO)_2Cu·H_2O$ (10 mg, 0.050 mmol) was stirred in DMF (3 mL). Then, TPyP (5 mg, 0.0081 mmol) and CF_3COOH (150 μL, 9.0 mmol) were sequentially added. After stirring the mixture for 5 minutes, it was placed in room temperature for three days, resulting in the formation of purple platelet-like crystals of **Cu-CuTPyP** (61.84% yield based on TPyP). **Cu-CuTPyP** ($C_{44}H_{24}Cu_2F_6N_8O_4$, M = 969.79): calcd. C: 54.49, H: 2.47, N: 1.16, O: 6.60; found C: 53.20, H: 2.57, N: 1.13, O: 6.49.

Preparation of films

The **$Cu_{14}I_{14}$-CuTPyP@PVDF** film (60 wt% loadding) was prepared via a spin coating method. 0.15 g **$Cu_{14}I_{14}$-CuTPyP** and 0.10 g polyvinylidene fluoride (PVDF, Mw ~ 534000) were dispersed in DMF (0.9 g). The mixture was stirred for 8 hours and then allowed to defoam for 24 hours. The resulting solution was dropped onto the center of a glass sheet and placed in the spin coating machine. It was spun at 2000 rpm/min for 1 minute and then immersed in ultra-pure water to remove the film. Finally, the $Cu_{14}I_{14}$-CuTPyP@PVDF film was obtained by drying it in an oven at 60 °C for 1 hour.

The preparation of **PVDF**, **TPyP@PVDF** and **Cu-CuTPyP@PVDF** films were consistent with the above method.

Table S1. Crystal data and structure refinements of **$Cu_{14}I_{14}$-CuTPyP** and **Cu-CuTPyP**.

	$Cu_{14}I_{14}$-CuTPyP	Cu-CuTPyP
CCDC number	2314637	2314638
Empirical formula	$C_{80}H_{48}Cu_{16}I_{14}N_{16}$	$C_{44}H_{24}Cu_2F_6N_8O_4$
Formula weight	4026.58	969.79
Temperature / K	200.01(10)	200.01(10)
Crystal system	monoclinic	monoclinic
Space group	I2/m	P2/m
a / Å	14.7545(2)	9.3379(5)
b / Å	16.6502(2)	13.8422(6)
c / Å	22.6488(3)	11.4183(5)
α / °	90	90
β / °	91.1210(10)	97.446(4)
γ / °	90	90
Volume / Å^3	5562.96(12)	1463.45(12)
Z	2	1
ρ_{calc} g / cm^3	2.404	1.100
μ/mm^{-1}	34.058	1.401
F(000)	3692.0	488.0
Crystal size / mm^3	0.2 × 0.15 × 0.05	0.2 × 0.1 × 0.02
Radiation	Cu Kα (λ = 1.54184)	Cu Kα (λ = 1.54184)
2Θ range for data collection / °	6.59 to 133.186	6.386 to 156.644
Index ranges	-17 ≤ *h* ≤ 17, -19 ≤ *k* ≤ 19, -26 ≤ *l* ≤ 23	-11 ≤ *h* ≤ 11, -17 ≤ *k* ≤ 16, -8 ≤ *l* ≤ 14
Reflections collected	17610	9707
Independent reflections	5082 [R_{int} = 0.0580, R_{sigma} =	2983
Data / restraints / parameters	5082 / 6 / 309	2983 / 30 / 200
Goodness-of-fit on F^2	1.081	1.079
Final *R* indexes [I >= 2σ (I)]	R_1 = 0.0625, wR_2 = 0.1823	R_1 = 0.0803, wR_2 = 0.2381
Final *R* indexes [all data]	R_1 = 0.0644, wR_2 = 0.1856	R_1 = 0.0891, wR_2 = 0.2448
Largest diff. peak/hole / e Å^{-3}	2.58/-2.48	0.98/-0.64

$R_1 = \sum||F_o|-|F_c||/\sum|F_o|$ $wR_2 = [\sum w(F_o^2 - F_c^2)^2/\sum w(F_o^2)^2]^{1/2}$

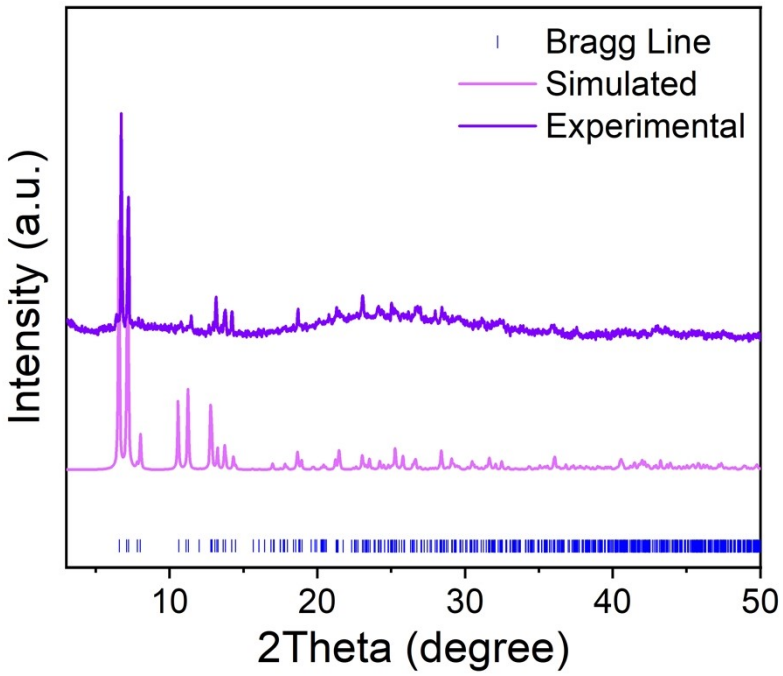

Fig. S1 The bragg lines of **$Cu_{14}I_{14}$-CuTPyP** (blue line), theoretical PXRD pattern (pale purple line), and experimental PXRD pattern (dark purple line).

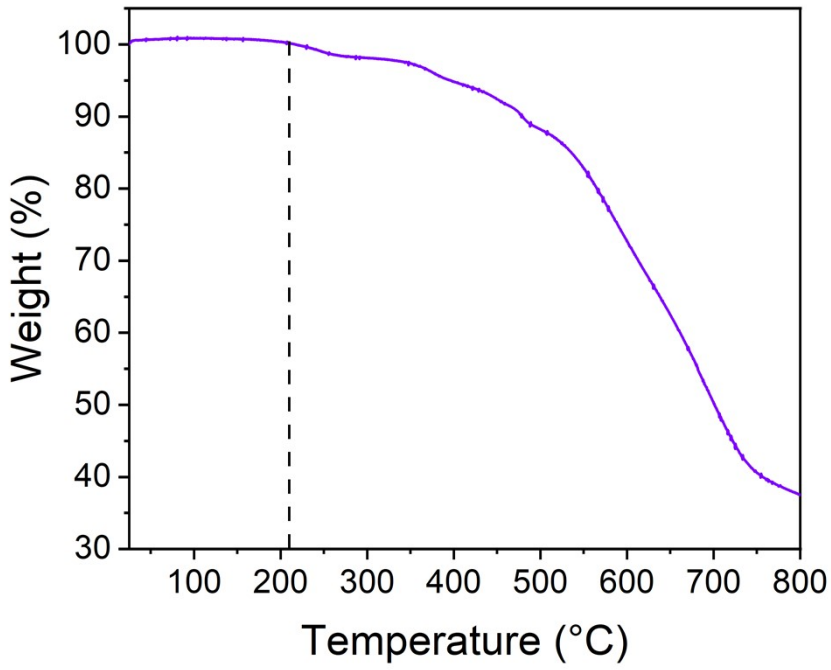

Fig. S2. The thermogravimetric analysis (TGA) curve of **$Cu_{14}I_{14}$-CuTPyP**.

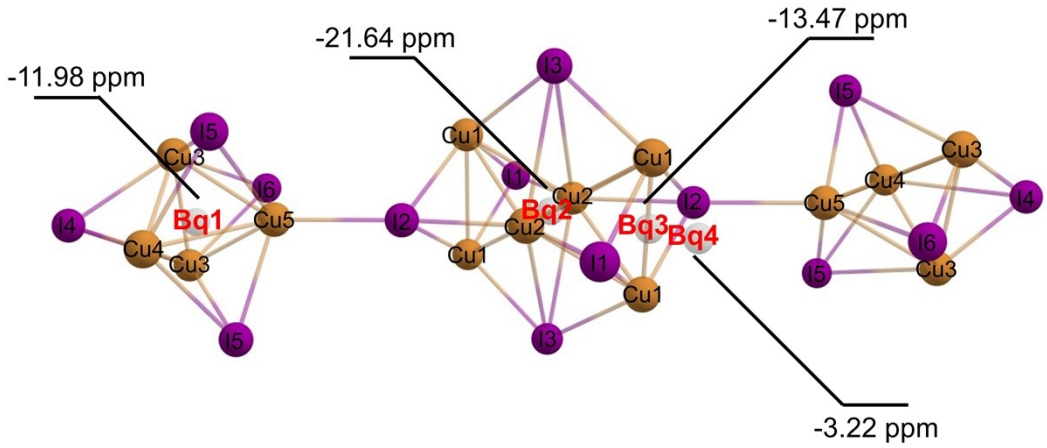

Fig. S3 The positions of the four ghost atoms (Bq1, Bq2, Bq3, Bq4) selected within the **$Cu_{14}I_{14}$** core, along with the calculated NICS values for positions Bq1-4.

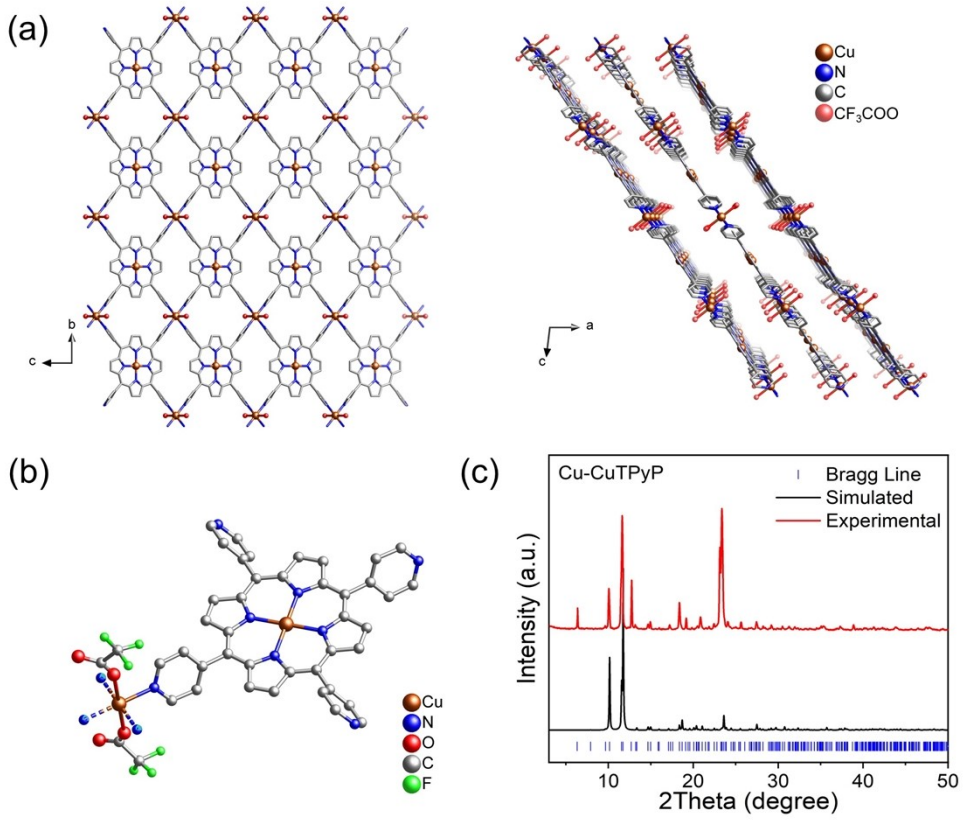

Fig. S4 (a) a-Axis and b-Axis crystal structures of **Cu-CuTPyP**. (b) The asymmetric structural unit of **Cu-CuTPyP**. (c) The bragg lines of **Cu-CuTPyP** (blue line), theoretical PXRD pattern (black line), and experimental PXRD pattern (red line).

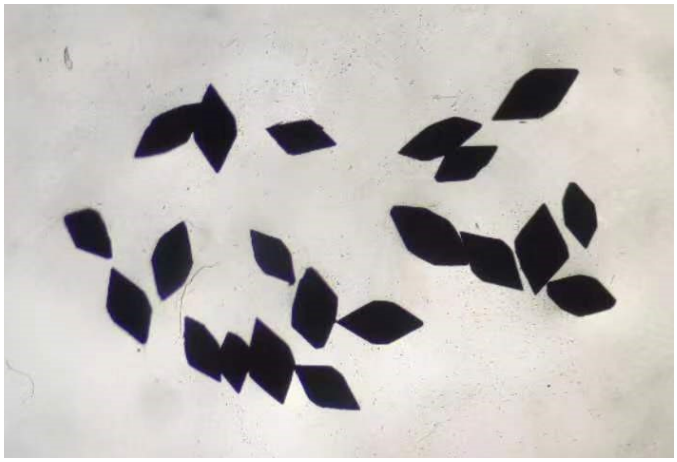

Fig. S5 Optical microscope image of crystalline samples of **$Cu_{14}I_{14}$-CuTPyP**.

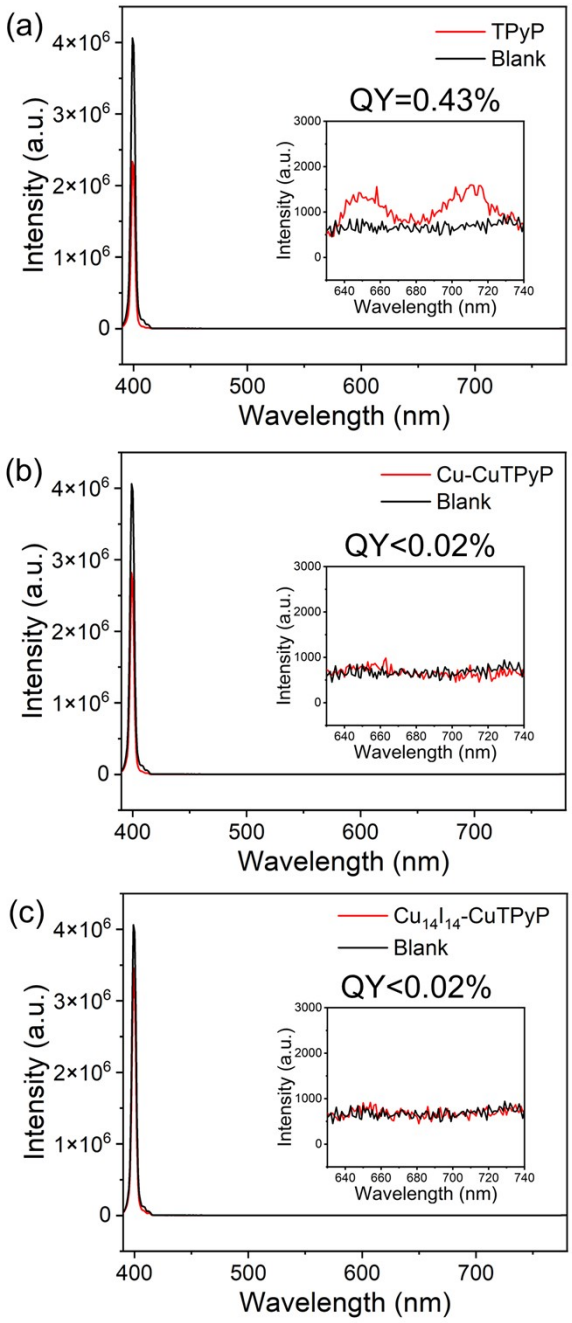

Fig. S6. Fluorescence emission spectra of **TPyP**, **Cu-CuTPyP** and **$Cu_{14}I_{14}$-CuTPyP** dispersed in EtOH excited at 400 nm for fluorescence quantum yield measurements.

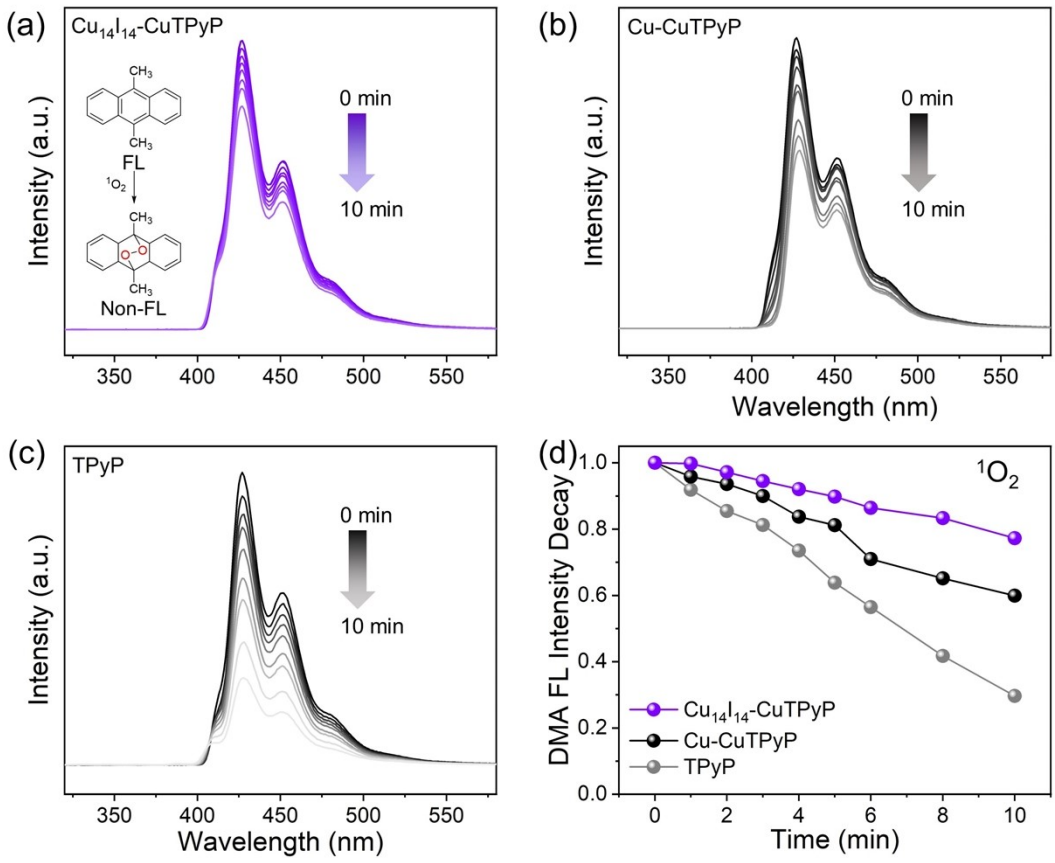

Fig. S7 Fluorescence emission spectrum of DMA in the presence of (a) **$Cu_{14}I_{14}$-CuTPyP**, (b) **Cu-CuTPyP**, and (c) **TPyP** under irradiation. (d) Decay curves of fluorescence intensity at 430 nm of DMA over illumination time in the presence of **$Cu_{14}I_{14}$-CuTPyP** (purple line), **Cu-CuTPyP** (black line), and **TPyP** (gray line).

Table S2. Comparison of the photothermal conversion efficiency (η) among various materials.

Classification	Contrast Sample	Light source	η (%)	Ref.
Porphyrin analogues (Organic materials)	YbL@MSN (Yb-carbazole-containing porphyrinoid complexes)	690 nm	45%	[4]
	Ni-1@DSPE (Ni(II) benzitripyrrin)	785 nm	45%	[5]
	TMPyP (a cationic porphyrin)	730 nm	59.3%	[6]
Nanoparticles (Inorganic materials)	Cu_9S_5 NPs	808 nm	25.7%	[7]
	CuS NPs	808 nm	28.8%	[8]
Porphyrin-based MOFs	TCPC-UiO MOF	635 nm	25.2%	[9]
	PB@UiO-66@TCPP MOF	808 nm	29.9%	[10]
	Ze-FeP MOF	635 nm	33.7%	[11]
	Au-Por MOF	808 nm	53.6%	[12]
	Pd-MOF	808 nm	27.7%	[13]
	$Cu_{14}I_{14}$-CuTPyP	1064 nm	63.77%	This work

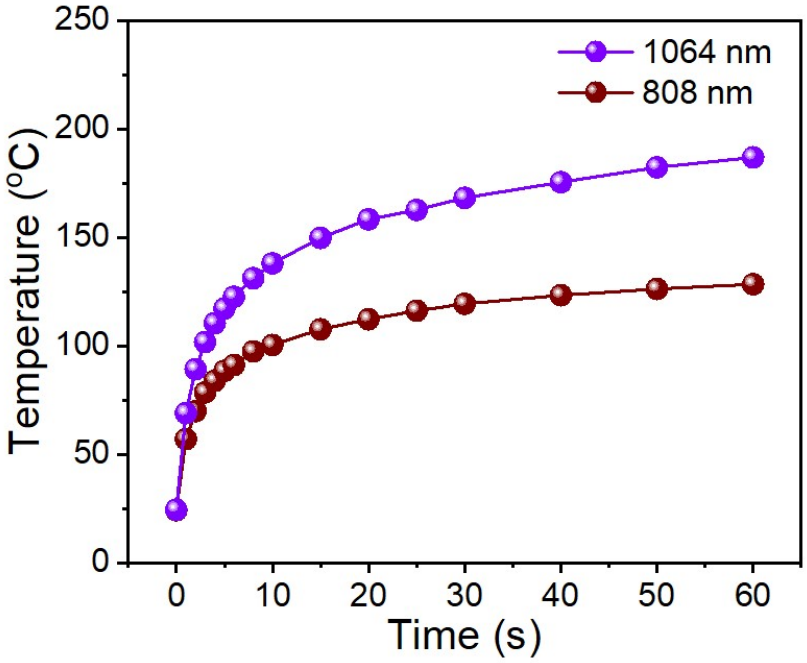

Fig. S8 Photothermal conversion curves of **$Cu_{14}I_{14}$-CuTPyP** under irradiation with a 1064 nm (purple line) or 808 nm (red line) laser (0.5 W cm^{-2}).

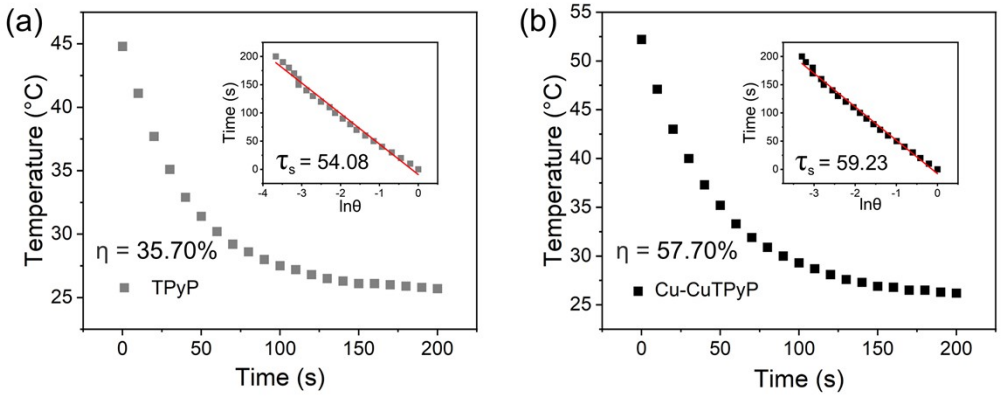

Fig. S9 Cooling curve of the quartz glass backside loaded with the **TPyP** and **Cu-CuTPyP** film after irradiation with a 1064 nm laser (0.5 W cm^{-2}), and its corresponding time-lnθ linear curve.

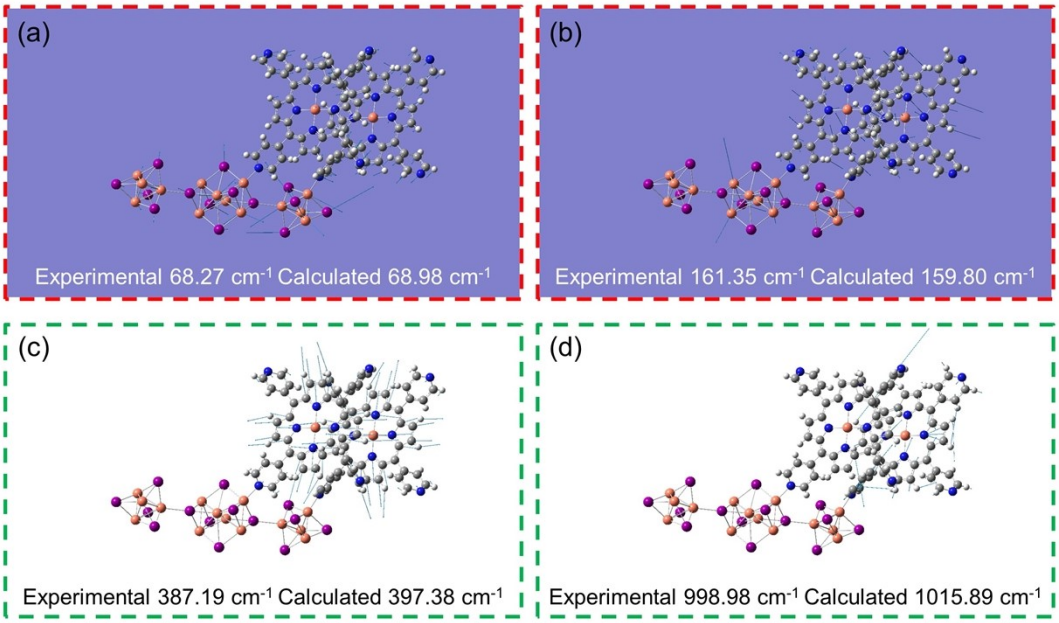

Fig. S10 Calculated molecular motions for some vibrational bands of **$Cu_{14}I_{14}$-CuTPyP**.

Table S3 Raman active modes of frequencies (in cm^{-1}) of the **$Cu_{14}I_{14}$-CuTPyP** for assignments. The calculations were carried out at the PBE1PBE/def2-SVP level of the DFT.

Observed frequency (cm^{-1})	Calculated frequency (cm^{-1})	Assignments
68.27	68.98	Stretching of the Cu-I and the Cu-Cu bands and translational motion of the pyridine and pyrrole rings
161.35	159.80	Stretching of the Cu-I and Cu-Cu bands and bending deformation of the pyridine rings and pyrrole rings
387.19	397.38	Stretching of the N-Cu bands in porphyrin rings, with expansion of the pyrrole (primarily) and pyridine (in opposite direction) rings
998.98	1015.89	Stretching of the C-C and C-N bands in pyrrole rings, in-plane bending deformation of the pyridine rings and rocking of the H on the C atoms in the pyridine rings

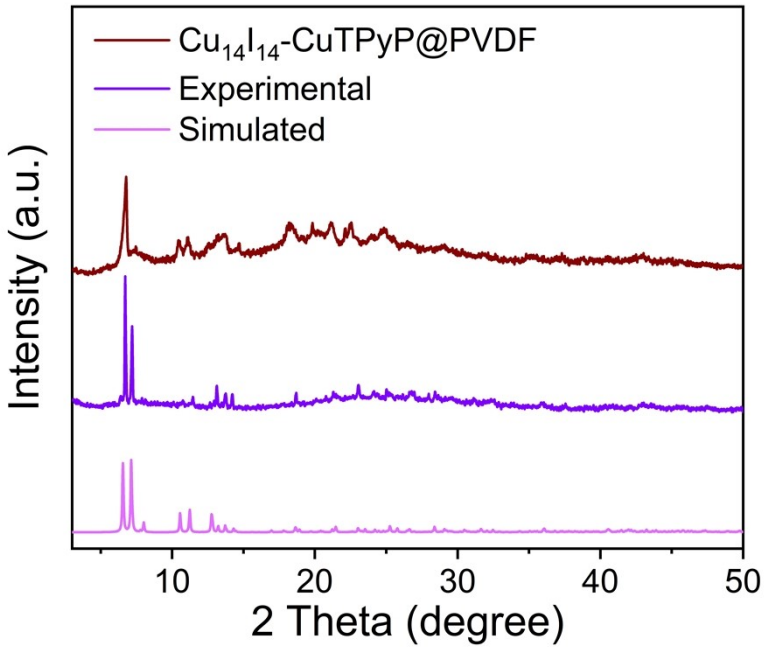

Fig. S11 Theoretical PXRD pattern (pale purple line) and experimental PXRD pattern (dark purple line) of **$Cu_{14}I_{14}$-CuTPyP**, experimental PXRD pattern of **$Cu_{14}I_{14}$-CuTPyP@PVDF**.

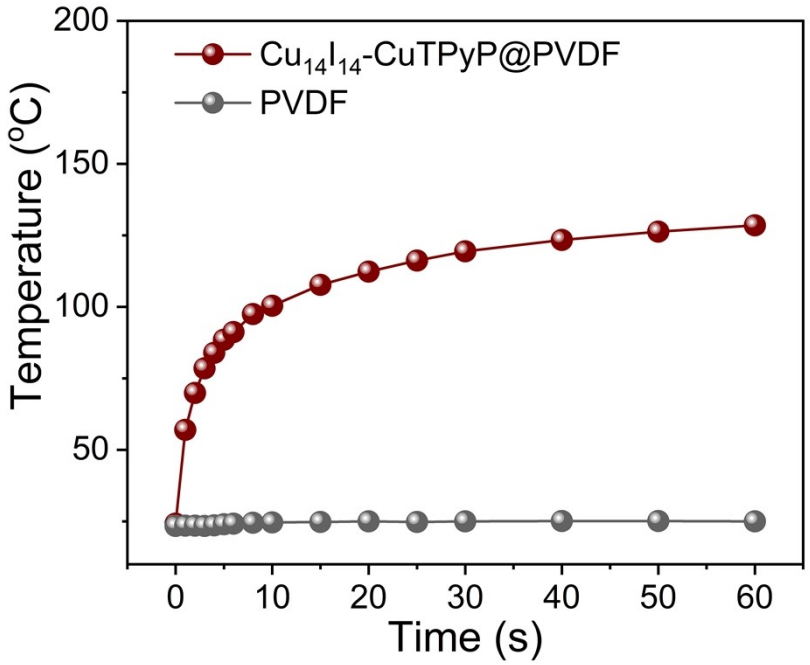

Fig. S12 Photothermal conversion curves under 1064 nm laser irradiation (0.5W cm^{-2}) of **$Cu_{14}I_{14}$-CuTPyP@PVDF** (rufous line) and **PVDF** (gray line) film.

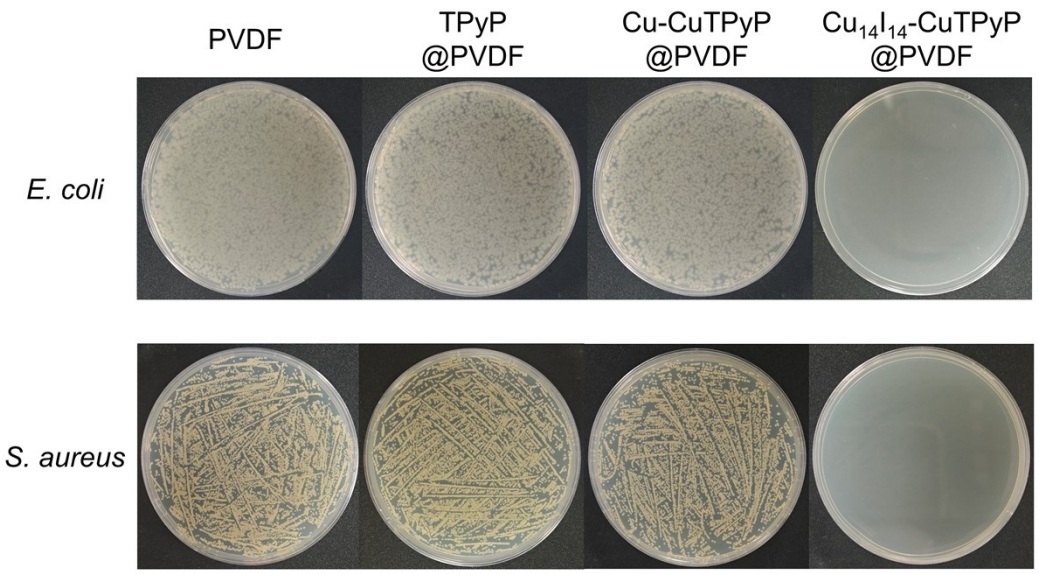

Fig. S13 Photos of plate count agars spread with *E. coli* and *S.aureus* after photothermal disinfection (irradiation with 1064 nm laser, 0.2 W cm^{-2}) using **PVDF**, **TPyP@PVDF**, **Cu-CuTPyP@PVDF** and **$Cu_{14}I_{14}$-CuTPyP@PVDF** films.

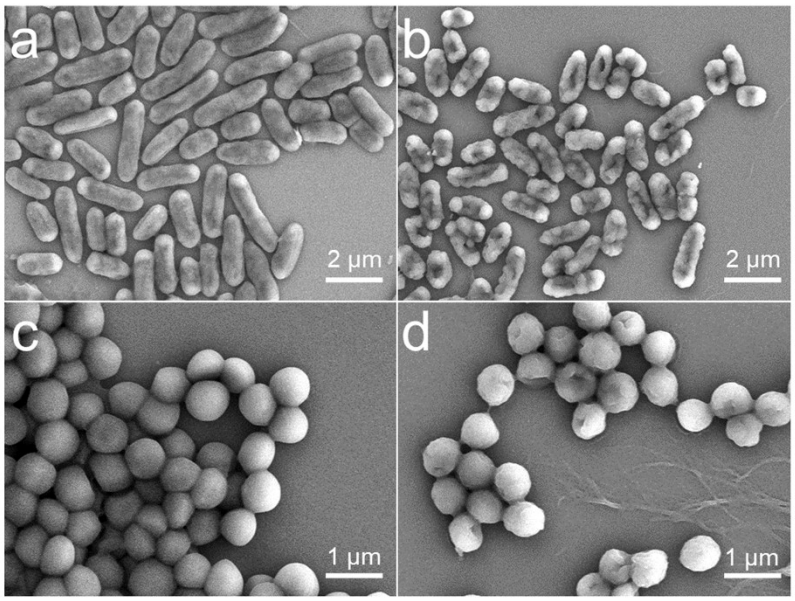

Fig. S14. SEM images of *E. coli* (a) before and (b) after, and *S. aureus* (c) before and (d) after photothermal disinfection with **$Cu_{14}I_{14}$-CuTPyP@PVDF** film.

Supplementary References

[1] J. P. Perdew, K. Burke, M. Ernzerhof, *Phys. Rev. Lett.* **1996**, *77*, 3865.

[2] H. J. Monkhorst, J. D. Pack, *Phys. Rev. B* **1976**, *13*, 5188.

[3] B. Lu, Y. Chen, P. Li, B. Wang, K. Mullen, M. Yin, *Nat. Commun.* **2019**, *10*, 767.

[4] M. Zhu, H. Zhang, G. Ran, D. N. Mangel, Y. Yao, R. Zhang, J. Tan, W. Zhang, J. Song, J. L. Sessler, J. L. Zhang, *J. Am. Chem. Soc.* **2021**, *143*, 7541-7552.

[5] Y. Yao, G. Ran, C. L. Hou, R. Zhang, D. N. Mangel, Z. S. Yang, M. Zhu, W. Zhang, J. Zhang, J. L. Sessler, S. Gao, J. L. Zhang, *J. Am. Chem. Soc.* **2022**, *144*, 7346-7356.

[6] H. Hu, H. Wang, Y. Yang, J. F. Xu, X. Zhang, *Angew. Chem. Int. Ed.* **2022**, *61*, e202200799.

[7] Q. Tian, F. Jiang, R. Zou, Q. Liu, Z. Chen, M. Zhu, S. Yang, J. Wang, J. Wang, J. Hu, *ACS Nano* **2011**, *5*, 9761-9771.

[8] H. Liu, J. Li, X. Liu, Z. Li, Y. Zhang, Y. Liang, Y. Zheng, S. Zhu, Z. Cui, S. Wu, *ACS Nano* **2021**, *15*, 18505-18519.

[9] X. Zheng, L. Wang, M. Liu, P. Lei, F. Liu, Z. Xie, *Chem. Mater.* **2018**, *30*, 6867-6876.

[10] Y. Luo, J. Li, X. Liu, L. Tan, Z. Cui, X. Feng, X. Yang, Y. Liang, Z. Li, S. Zhu, Y. Zheng, K. W. K. Yeung, C. Yang, X. Wang, S. Wu, *ACS Cent. Sci.* **2019**, *5*, 1591-1601.

[11] K. Zhang, X. Meng, Y. Cao, Z. Yang, H. Dong, Y. Zhang, H. Lu, Z. Shi, X. Zhang, *Adv. Funct. Mater.* **2018**, *28*, 1804634.

[12] G. Zhou, Y. Chen, W. Chen, H. Wu, Y. Yu, C. Sun, B. Hu, Y. Liu, *Small* **2023**, *19*, e2206749.

[13] G. Zhou, Y. S. Wang, Z. Jin, P. Zhao, H. Zhang, Y. Wen, Q. He, *Nanoscale Horiz.* **2019**, *4*, 1185.